國立臺灣大學工學院化學工程學系

碩士論文

Department of Chemical Engineering
College of Engineering
National Taiwan University
Master Thesis

彈性體之拉伸強度與韌性的最佳交聯密度:
交聯與纏結之間的競爭

Optimal Crosslinking Density of Elastomer for Tensile Strength and Toughness: Competition between Crosslinking and Entanglement

蘇庭瑜

Ting-Yu Su

指導教授: 謎玉真 博士

Advisor: Yu-Jane Sheng, Ph.D.

中華民國 112 年 6 月

June, 2023

doi:10.6342/NTU202301105

國立臺灣大學碩(博)士學位論文
口試委員會審定書

彈性體之拉伸強度與韌性的最佳交聯密度：交聯與纏結之間的競爭
Optimal Crosslinking Density of Elastomer for Tensile Strength and Toughness: Competition between Crosslinking and Entanglement

本論文係蘇庭瑜君（R10524005）在國立臺灣大學化學工程學系、所完成之碩（博）士學位論文，於民國 112 年 06 月 15 日承下列考試委員審查通過及口試及格，特此證明

口試委員：

謝之真 （簽名）

（指導教授）

曹恆光

黃俊仁

陳貴賢

系主任、所長 廖英志 （簽名）

（是否須簽章依各院系所規定）

誌謝

經歷研究所兩年的磨練，讓我更加了解分子模擬在化工上的廣泛應用，首先要特別感謝我的指導老師謝玉真教授以及曹恆光教授，在每次的開會討論，給予我許多寶貴的意見與想法，並有條不紊地為我指點迷津，而讓論文研究順利完成。我非常感謝在碩士班所學習的一切，也讓我找到自己的專長以及興趣，我會在未來繼續專研化工產業最新的趨勢，將所學的知識都應用在生活上。不僅僅要成為一位知識接受者，更要變成一位知識傳播者。取之於社會，用之於社會。

很感謝電腦分子模擬實驗室的所有成員，冠郁、心瑀、昱浩、明璋、昕緯、宜庭、冠臨、千又、致融、斯楷、雅雯、習鈞、慧新，以及中央實驗室的同學，我要特別謝謝明璋與致融，平時不厭其煩地與我討論實驗上的細節以及程式上的修正等，感謝大家平時在實驗上給我的意見，並給予我照顧以及鼓勵，雖然相處的時間不是很長，但我非常開心能與大家相遇及認識。謝謝實驗室所提供的資源，時常舉辦許多活動，像是實驗室出遊、導生宴、尾牙等等，讓我感到十分幸福與溫暖。在論文口試期間，承蒙黃俊仁教授以及陳儀帆教授撥冗審閱論文及指正，給予我許多寶貴的建議，並使論文內容更加豐富與完善，在此致上最真摯的感謝與祝福。

最後，我要感謝我最珍愛的家人，謝謝你們讓我能夠無後顧之憂，專心完成碩士班學業，在我感到迷惘時，給予我關心與包容。沒有你們就沒有今天的我，謝謝你們的支持與鼓勵，讓我能順利完成這份論文，我想將這份喜悅分享給大家。謝謝在求學路上，幫助過我的所有貴人，謝謝每個人對我的指導以及給我的寶貴意見，我會銘記在心。如同蘭道所說:「科學如同大海，要求奮不顧身的拼搏。」人生亦是如此，需要靠努力的奮鬥來克服困難與恐懼，正是因為有了風雨的洗禮才能看見斑斕的彩虹。期許自己在未來不管遇到什麼樣的挑戰，依舊能夠樂觀向上，不被困難所擊敗，化阻力為助力，並從瓶頸中突破自我。

doi:10.6342/NTU202301105

摘要

交聯通常可以提升高分子的機械性能，然而已有研究指出一些機械性能的表現會隨著交聯劑濃度的增加呈現非單調的變化，但這些行為背後的機制卻尚未被完全理解。因此，本研究使用耗散粒子動力學的模擬方法，探討交聯程度對交聯分支高分子系統之機械特性影響。除了探究應力-應變曲線外，亦透過測量凝膠含量、結晶度和微觀結構等微觀特性來深入了解彈性體的結構-性能關係。研究結果如預期所示，交聯程度的增加會導致結晶度降低，但是凝膠含量會提高。此外，隨著交聯劑濃度的增加，楊氏模數會上升，而斷裂伸長量會下降。不同的是，抗拉強度和韌性會隨交聯程度的增加，而呈現先增加後穩定下降的趨勢。交聯高分子的微觀結構特性可以透過平均鍵長($\bar{l}_b$)以及高分子迴轉半徑($\overline{R}_g$)來分析，隨著交聯劑濃度的增加，斷裂處的平均鍵長會一開始增加，但在最適濃度後會趨於飽和，而斷裂處的平均高分子迴轉半徑則會逐漸下降。這些研究結果顯示，抗拉強度和韌性的最大值是交聯和纏結之間競爭的結果。

關鍵字: 彈性體；分子模擬；交聯密度；應力-應變曲線

doi:10.6342/NTU202301105

ABSTRACT

Crosslinking generally enhances the mechanical properties of crosslinked polymers. However, some mechanical properties have been reported to vary non-monotonically with the concentration of crosslinkers, and the underlying mechanism for this behavior is not yet fully understood. In this work, the effect of the crosslinking degree on the mechanical characteristics of the crosslinked systems made of branched polymers are explored by dissipative particle dynamics simulations. In addition to the stress-strain curve, the microscopic characteristics of the elastomer, such as the gel content, crystallinity, and microstructure, are obtained to gain insights into the structure-property relationship. As expected, an increase in the degree of crosslinking leads to a decrease in the degree of crystallinity, but an increase in the gel content. Moreover, the Young's modulus increases with the crosslinker concentration, while the elongation at break decreases. In contrast, the tensile strength and toughness initially increase and then steadily decrease as the crosslinking degree increases. The microstructural characteristics are analyzed based on average bond length ($\bar{l}_b$) and radius of gyration of polymers ($\bar{R}_g$). As the crosslinker concentration increases, $\bar{l}_b$ at break grows initially but becomes saturated beyond the optimal concentration, while $\bar{R}_g$ at break always decreases. Our findings suggest that the maxima in tensile strength and toughness are the consequence of the competition between crosslinking and entanglement.

Keywords: Elastomer; Molecular simulation; Crosslinking density; Stress-strain curve

doi:10.6342/NTU202301105

CONTENTS

doi:10.6342/NTU202301105

LIST OF FIGURES

doi:10.6342/NTU202301105

Chapter 1 Introduction

Linear low-density polyethylene (LLDPE) is a type of polyethylene that is made by copolymerizing ethylene with a small amount of an alpha-olefin, such as butene or hexane [1-3]. LLDPE has a linear structure with short side chains, which gives it a lower density and greater toughness compared to traditional high-density polyethylene (HDPE). It is lightweight and cost-effective, and exhibits excellent resistance to impact and chemicals, making it suitable for use in packaging films and wire and cable insulation, among other applications [4-7]. Additionally, LLDPE is easy to process using various conventional thermoplastic processing techniques such as blow molding and extrusion, which enables the production of intricate shapes and structures [8, 9]. However, in certain applications, such as insulation, the mechanical strength of LLDPE may not be sufficient, and therefore, a chemical crosslinking process may be introduced to create stronger and more stable bonds between the polymer chains [10]. That is, LLDPE is crosslinked by chemical crosslinking agents to obtain crosslinked LLDPE (XLPE), which typically exhibits higher mechanical strength, including improved resistance to deformation under stress, greater impact resistance, and higher tensile strength [11].

The mechanical properties of XLPE, such as Young's modulus, tensile strength, and toughness, depend on the type of crosslinker and the network structure (gel content). The latter varies strongly with the crosslinking density (the crosslinker concentration). That is, their mechanical properties can be effectively tailored by controlling the crosslinking density of the network for a chosen crosslinker [12]. Intuitively, increasing the crosslinking density of crosslinked polymers leads to an improvement in their mechanical strength. However, previous studies have primarily focused on crosslinked polymers with low crosslinking density [13-15], because higher crosslinking densities do not necessarily

doi:10.6342/NTU202301105

result in better mechanical strength. For example, when using dicumyl peroxide (DCP) as a crosslinker for LLDPE or silane grafted LLDPE, it has been found that as the concentration of crosslinker increases, the elongation at break (extensibility) decreases, but the tensile strength reaches its maximum value at a certain DCP concentration [16, 17]. Similarly, when bis(tert-butyldioxyisopropyl)benzene-hexane (BIPB) is used as a crosslinker for HDPE, the impact strength - an important measure of material toughness - reaches its maximum value at a specific BIPB content [18].

The degree of crosslinking is well-known to play a crucial role in determining the mechanical properties of crosslinked polymers, such as their stiffness and toughness [19, 20]. Numerous experimental studies have investigated the correlation between crosslinking density and mechanical properties in various polymers, including LLDPE, HDPE, and polyurethanes [21-23]. Unfortunately, the reason for the optimal concentration of crosslinker required to achieve maximum mechanical properties is still not fully understood. Furthermore, the microscopic mechanism underlying this phenomenon is difficult to observe experimentally but may be elucidated through molecular simulations, which are currently lacking. Recently, the mechanical characteristics of polymers in which entanglements greatly outnumber crosslinks have been reported [24]. The effects of the crosslinker-to-monomer molar ratio (C) on the stiffness and toughness of highly entangled poly(ethyl acrylate) elastomers are investigated. The stiffness of the elastomer reaches a plateau beyond $C \sim 10^{-6}$, and it starts to increase again after C reaches around 10^{-3}. The presence of entanglements has been proposed as the reason for the stiffness plateau, while the gradual increment in stiffness after the plateau is attributed to the dense enough cross-links prevailing over entanglements. In contrast, it is found that the toughness decreases as the crosslinking density (C) increases. When the elastomers have the low crosslinking density (C), the

doi:10.6342/NTU202301105

entanglements are dense, and cross-links are sparse. This results in higher toughness since the entanglements do not hinder the transmission of tension along the long polymer chains [24].

The tensile strength and toughness of crosslinked polymers (e.g., chemical elastomer) are found to vary non-monotonically with the concentration of crosslinkers [16, 17]. In fact, an optimal crosslinking density exists for achieving the maximum tensile strength or toughness. Unfortunately, the underlying mechanism, particularly the microscopic insight, is still elusive. The objective of this study is to investigate the effect of the crosslinking degree on the mechanical and microstructural properties of the crosslinked system made of branched polymers under uniaxial extension, using coarse-grained dissipative particle dynamics (DPD). Molecular simulations offer several advantages over traditional experimental approaches for studying the properties of polymer networks due to better control of network formation and accurate knowledge of network features [25]. In order to ensure that the branched polymers are in the solid state, the transition from liquid to solid state of non-crosslinked branched polymers is analyzed through measurements of crystallinity and heat capacity. The gel content of the crosslinked polymer is determined for various degrees of crosslinking. Uniaxial stretching is used to acquire the stress-strain curve for different degrees of crosslinking. The mechanical properties of the crosslinked polymers, such as Young's modulus (E), elongation at break, tensile strength, and toughness, are then evaluated based on the acquired data. Lastly, the microstructural dynamics are captured by monitoring the evolution of the average bond length $\bar{l}_b(t)$ and average radius of gyration of polymers $\bar{R}_g(t)$. The effect of the competition between microscopic characteristics of networks, specifically crosslinking points and chain entanglements, on the mechanical properties of crosslinked polymers are discussed.

doi:10.6342/NTU202301105

Chapter 2 Method

2.1 Simulation method and model

DPD is a coarse-grained molecular dynamics method that utilizes a stochastic DPD thermostat to conserve total momentum and employs soft potentials mapped onto the classical lattice Flory-Huggins theory [26, 27]. It is a particle-based mesoscale simulation that enables the investigation of larger length and time scales compared to conventional molecular dynamics (MD) [27-29]. The DPD bead, which has a mass of m, consists of several molecules or atoms, and its time evolution is governed by Newton's equations of motion [30, 31]. The interactions between DPD beads involve pairwise conservative force (f_{ij}^{C}), dissipative force (f_{ij}^{D}) and random force (f_{ij}^{R}): $F_i = \sum_{j(\neq i)} (f_{ij}^{C} + f_{ij}^{D} + f_{ij}^{R})$. The forces are short-ranged, soft, and repulsive in nature [27]. All the bead-bead interactions are characterized by a finite cutoff distance, denoted as r_c, which is usually taken as the unit of length. All units in DPD simulations are scaled by the bead mass (m), cut-off distance (r_c), and thermal energy (k_BT) [32]. Thereby, the time (t) is scaled by $(mr_c^2/k_BT)^{1/2}$ and the stress (τ_{ij}) scaled by k_BT/r_c^3.

The conservative force decays linearly with the inter-bead distance (r_{ij}), $f_{ij}^{C} = a_{ij}(1 - r_{ij}/r_c)\hat{r}_{ij}$, where the unit vector $\hat{r}_{ij}$ is along the direction of the inter-bead distance. The interaction parameter a_{ij} represents the maximum strength of the repulsive force between beads i and j. a_{mm} associated with any two beads of the same component is set to $a_{mm} = 25$ [33, 34]. For simplicity, one assumes that the monomers and crosslinkers belong to the same component. The dissipative force (f_{ij}^{D}) acts as the friction between the beads and is proportional to the relative velocity between them. On the other hand, the random force (f_{ij}^{R}) acts as a source of heat and is added to satisfy the fluctuation-

doi:10.6342/NTU202301105

dissipation theorem [34-37]. The conservation of momentum is automatically fulfilled in DPD, and the hydrodynamic behavior of the system can be observed more easily compared to MD, which contains excessive details of molecular motion [38-40]. In this work, the open software Large-scale Atomic/Molecular Massively Parallel Simulator (LAMMPS) [41] is used for all DPD simulations.

Our simulation results mainly focus on the properties of branched and crosslinked polymers, in addition to linear polymers. A linear polymer is composed of repeating units connected to only two others [42]. In contrast, branch polymers have side chains growing out from the main chain [43], and crosslinked polymers have linkages between polymer chains [44]. In this work, both linear and branched polymers are modeled as a string of DPD beads, with each polymer chain consisting of a total of 130 beads. The branched polymer contains 6 short branches that are uniformly distributed along the backbone, with each branch consisting of one DPD bead. This is a simplified model to mimic the structure of butane-based LLDPE, which has short branches due to butane units. The neighboring beads in a polymer are connected with the harmonic spring, $F_{ij}^{S} = k_s(r_{ij} - r_{eq})\hat{r}_{ij}$, where the spring constant is $k_s = 100$ and the equilibrium length $r_{eq} = 0.4$. The chain stiffness can be controlled by introducing additional bending forces between two consecutive bonds, $F^{\theta} = -\nabla U^{\theta}$, where the bending potential is $U^{\theta} = k_{\theta}(\theta - \theta_{eq})^2$. k_{θ} represents the bending constant and θ_{eq} is the equilibrium angle between two consecutive bonds. Along the backbone, the bending constant is $k_{\theta} = 2$ and the equilibrium angle $\theta_{eq} = \pi$. However, to represent the free movement between the branch and the main chain, the bending constant is set to $k_{\theta} = 0$.

The simulation system contains more than 400 branched polymers which are randomly crosslinked by crosslinkers. Figure 1 depicts a schematic diagram of two

doi:10.6342/NTU202301105

branched polymers crosslinked by a crosslinker, which consists of two connected DPD beads and is actually a dimer of a linear polymer. The total number of beads is approximately 6×10^4 DPD beads and the bead (volume) fraction of crosslinkers varies from 0.5 to 10%. Note that all crosslinkers are attached to polymers, so the volume fraction of crosslinkers is equivalent to the degree of crosslinking of the network. The number density of the system is always maintained at $\rho = 3$. Without stretching, the system is a cubic box ($27.1 \times 27.1 \times 27.1$) with periodic boundary in all three spatial directions. A time step of $\Delta t = 0.01$ is used for the simulations, and it takes approximately 2×10^6 time steps for the system to reach equilibrium.

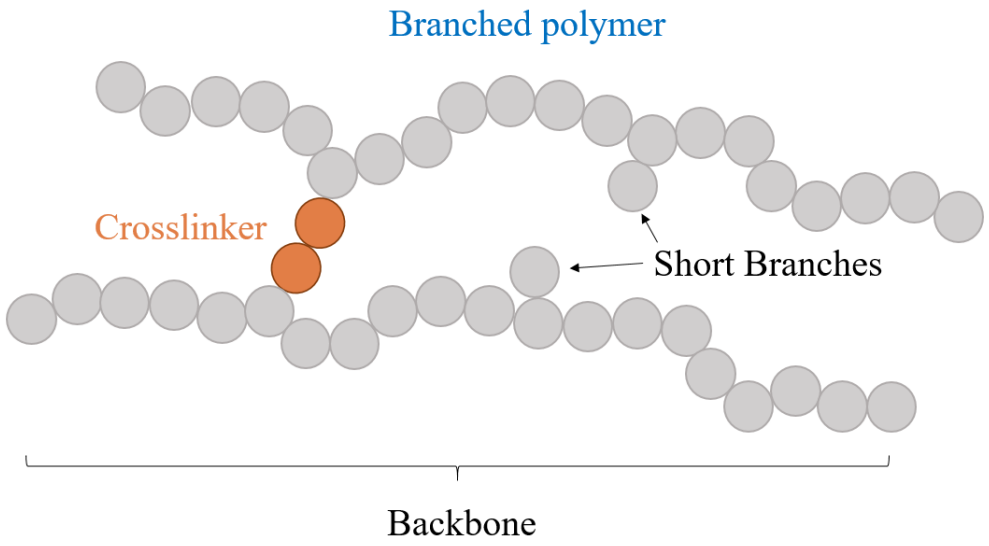

Figure 1. Schematic diagram of two branched polymers crosslinked by a crosslinker.

The original DPD parameters, as proposed by Groot and Warren [27], are too soft and do not enforce specific restrictions on steric interactions, potentially leading to chain crossings and phantom chains. However, an easy and computationally efficient criterion [45] was provided for imposing topological constraints, which gives the uncrossability of polymeric chains for DPD simulations. If the condition $\sqrt{2}r_{min} > l_{max}$ is satisfied

doi:10.6342/NTU202301105

throughout the simulation, chain crossings will not occur. Here r_{min} denotes the minimum value of nonbonded length and l_{max} is the maximum value of bond length. Therefore, selecting appropriate DPD parameters can maintain the uncrossability of polymeric chains. Recently, the criterion for the uncrossability of polymeric chains has been validated for the parameters of $r_{eq} = 0.4$, $k_s = 100$, and $a_{ij} = 25$. [32]. In this study, we choose the same DPD parameters to maintain the uncrossability of polymeric chains effectively, and at the same time, the large integration step can still be employed.

2.2 Thermodynamic properties

The crystallinity, heat capacity, gel content, and radius of gyration of polymers are calculated from the simulations. The crystalline domain is defined as a group of bonds with the same orientation in a specific region [46]. To determine whether a specific bond is in a crystalline state, the following rules are applied. First, consider a spherical domain with the center located at the midpoint of a selected bond that connects two consecutive beads i and $i + 1$ along the polymer chain. Next, determine the number of neighboring bonds that are collinear with the selected one. The radius of the domain is 1.0 DPD units and the collinearity threshold criteria is less than 26° for the spanned angle between two bonds. The ratio of collinear neighbors to the total number of neighbors is used as the criterion for bond crystallization. If this ratio is greater than 0.4, the bond is considered crystalline; otherwise it is classified as amorphous. The degree of crystallinity (α) is defined as the proportion of crystalline bonds relative to the total number of bonds in the system.

The heat capacity (C_v) of a material is closely related to its structure and can serve as a sensitive measure of the degree of order within a system [47, 48]. The structural

doi:10.6342/NTU202301105

phase transition can be detected by using calorimetry to observe the variation of the heat capacity with temperature [49]. In NVT (canonical ensemble) simulations, the evaluation of heat capacity involves determining the mean squared energy fluctuations at each temperature [50], $C_v = (\langle E^2 \rangle - \langle E \rangle^2)/k_B T^2$, where E represents the internal energy. The gel content is a crucial factor that affects the behavior and properties of crosslinked polymers, and it is commonly used to characterize the degree of crosslinking [51, 52]. In experiments, the gel content is determined by calculating the percentage of insoluble material remaining in the crosslinked polymer after solvent extraction, relative to the initial weight of the polymers. In simulations, the gel content is determined by calculating the percentage of the number of branched polymers associated with the largest cluster of crosslinked polymers, relative to the total number of branched polymers in the system, in a similar way to experimental measurements.

The crosslinked network is formed by linking together branched polymers with crosslinkers. In simulations, we are able to monitor the conformation of each branched polymer before and after crosslinking. During the stretching process, it is possible to track the conformational changes of crosslinked polymers within the network. The size and shape of a polymer are typically described by its radius of gyration (R_g), which provides information about its conformation [53]. The radius of gyration of a material is defined as the root mean square distance of each element within the body from its center of mass [54]. The size of a polymer along the x-axis can be expressed as $R_{gxx} = [\sum_{i=1}^{N} \frac{(x_i - x_{cm})^2}{N}]^{\frac{1}{2}}$, where x_{cm} represents the center-of-mass position. The radius of gyration of a polymer is written as $R_g = (R_{gxx}{}^2 + R_{gyy}{}^2 + R_{gzz}{}^2)^{1/2}$ [54]. The average radius of gyration of polymers is obtained by taking the mean of the R_g values for all the chains in the system.

doi:10.6342/NTU202301105

2.3 Mechanical properties

The stress-strain curve can be acquired by using simulation box deformation of LAMMPS. In the uniaxial extension simulation, all polymers are subjected to uniaxial stretching at a constant strain rate ($\dot{\varepsilon}$), and the resulting elongational stress (τ) is subsequently determined. The elongational stress in the system is defined as the normal pressure differences, $\tau = \tau_{xx} - (\tau_{yy} + \tau_{zz})/2$ [55]. The average virial stress, τ_{kk}, is calculated from the negative value of the diagonal component P_{kk} of the pressure tensor in the k direction [56]. The normal pressure (P_{kk}) is composed of two contributions, $P_{kk} = (\sum_i m^i v_k^i v_k^i /V) + 0.5(\sum_{(j\neq i)} F_k^{ij} r_k^{ij} /V)$, with V representing the volume of the simulation box. m^i and v_k^i correspond to the mass and k-component of the velocity of bead i. Additionally, F_k^{ij} and r_k^{ij} depict the k-component of the interacting force and the distance between beads i and j. The first term in P_{kk} pertains to the kinetic energy, while the second term is concerned with the potential energy [57]. After equilibration of the system, simulations of uniaxial-stress tensile deformation were carried out in the x-direction. A constant true strain rate of $\dot{\varepsilon} = 5 \times 10^{-4}$ is applied to the initial cubic box, causing the x-dimension box size to increase nonlinearly over time, which is denoted by $L_x(t) = L_0 \exp(\dot{\varepsilon}\Delta t)$. Here L_0 represents the initial box size and L_x the box size in the x-dimension at t. The deformation simulation is conducted under the constant volume condition, with the y- and z-dimensions of the box shrinking equally over time.

The tensile test is a common method for evaluating important mechanical properties of polymers, including Young's modulus, elongation at break, tensile strength, and toughness [58]. The Young's modulus can be obtained from the slope of stress-strain curve in the linearly elastic region [59]. Elongation at break denotes the strain of a material at the point of breakage, and it describes the material's ability to deform before

doi:10.6342/NTU202301105

failure. Tensile strength represents the maximum stress that a material can endure while being stretched before reaching its breaking point [60]. Additionally, the toughness is given by the area under a stress-strain curve, which measures the amount of energy absorbed by the material prior to its failure [61]. Although bond breakage or necking associated with stretching is not allowed in DPD simulations, the simulation can be terminated automatically if the system energy diverges due to the prolonged stretching of harmonic bonds. At the point of numerical divergence, the strain can be defined as the elongation at break, and the stress corresponds to the material's tensile strength.

doi:10.6342/NTU202301105

Chapter 3 Result and Discussion

3.1 Melting temperature, crystallinity, and gel content

To understand the crosslinking effects, the comparison must be made with respect to solid polymer without crosslinking. The solid state is ensured as the system temperature is below the melting temperature T_m, which can be determined from the variation of crystallinity or heat capacity with temperature. Figure 2a shows the plot of the degree of crystallinity against temperature for linear and branched polymers. Linear polymer is considered for the purpose of comparison. As expected, the degree of crystallinity is low ($\alpha \approx 0.05$) at higher temperature but grows rapidly as $T \rightarrow T_m$, corresponding to the transition from disordered melt to crystalline solid upon cooling. Here the melting temperature is defined as the temperature at which the degree of crystallinity is approximately the average value of the liquid and solid states. The morphology of polymers at different temperatures is demonstrated in Fig. 2b. As the temperature decreases, the more ordered structure begins to develop and the crystalline region (as highlighted within the yellow circle) grows accordingly. It is evident that both T_m and α of linear polymer are higher than those of branched polymer, consistent with previous studies [62-64]. This result is attributed to the fact that linear polymers are easier to align with each other and pack closely than branched polymers. Therefore, the former can crystallize at higher temperature and has a large amount of crystallinity than the latter.

doi:10.6342/NTU202301105

(a)

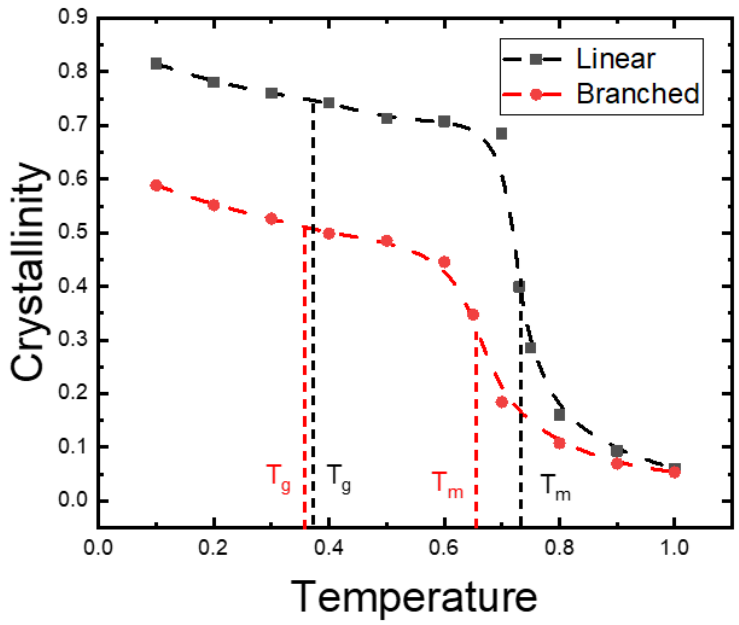

(b)

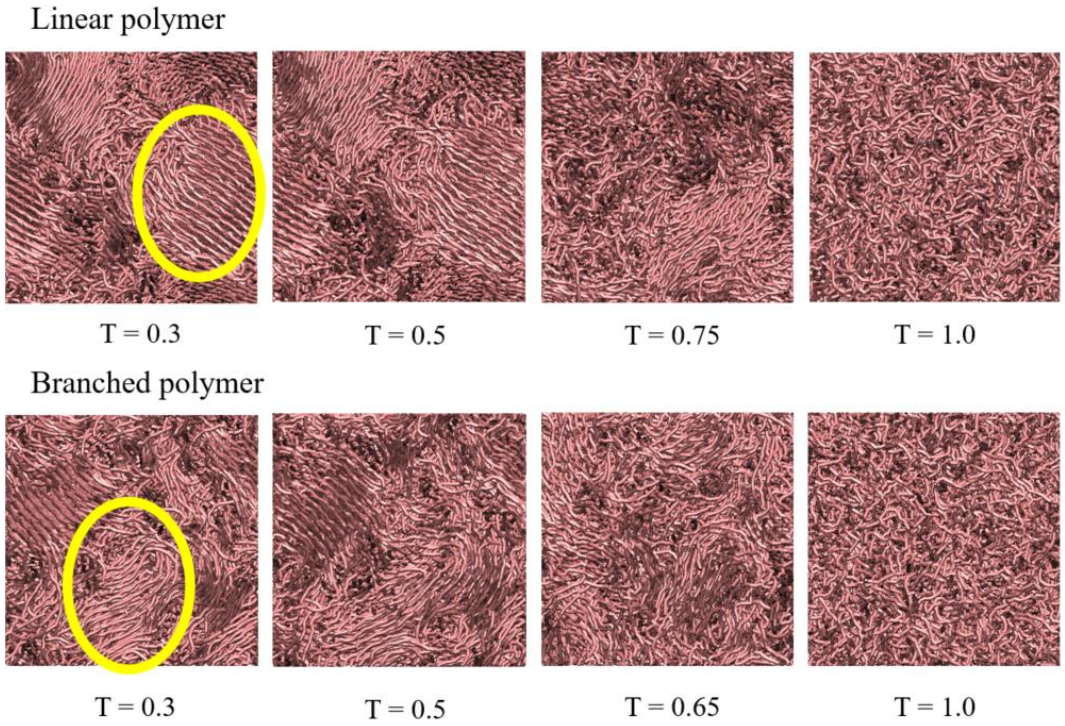

Figure 2. (a) The plot of the degree of crystallinity against dimensionless temperature for linear and branched polymers. (b) The morphology of linear and branched polymers at different temperature.

doi:10.6342/NTU202301105

In addition to the crystallinity, the heat capacity is also adopted to estimate the melting temperature, as shown in Fig. 3. The heat capacity (C_v) is corresponding to the mean squared fluctuations in internal energy at a specified temperature [65, 66]. T_m is the temperature at which C_v arrives at its maximum value, signifying change from the molten to solid state upon cooling. The melting temperatures of linear and branched polymers determined from the heat capacity curves (C_v vs. T) are essentially the same as those acquired from the crystallinity curves (α vs. T). In the C_v -T plot, the heat of melting (ΔU_m) can be estimated from the area under the peak. ΔU_m of linear polymer is significantly greater than ΔU_m of branched polymer. This consequence of the heat capacity is consistent with the result of the crystallinity, because more latent heat is required to destroy more crystalline regions formed in the solid state of linear polymer.

(a)

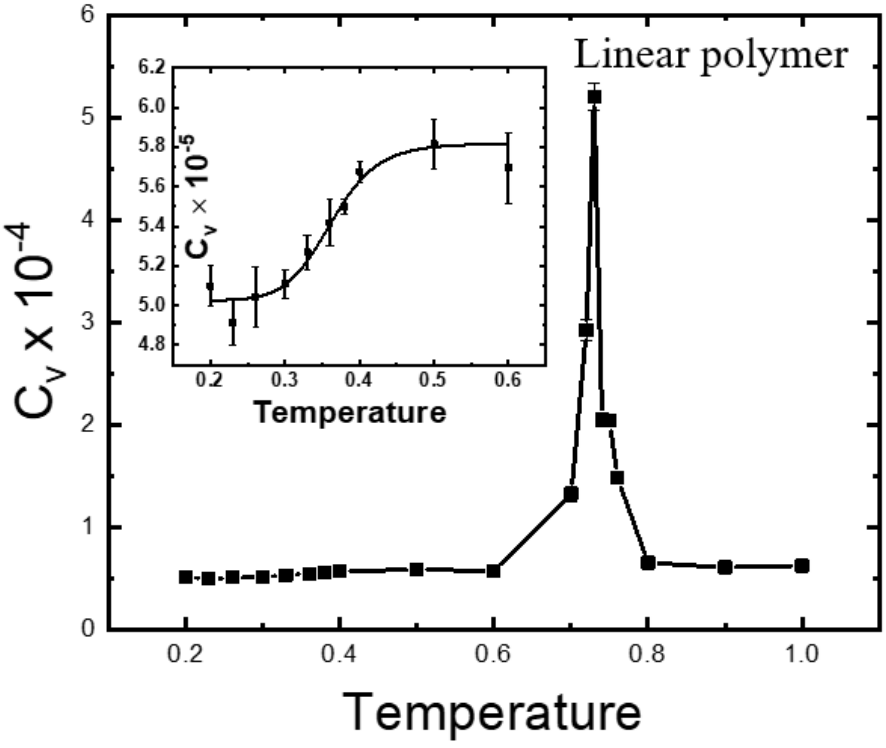

doi:10.6342/NTU202301105

(b)

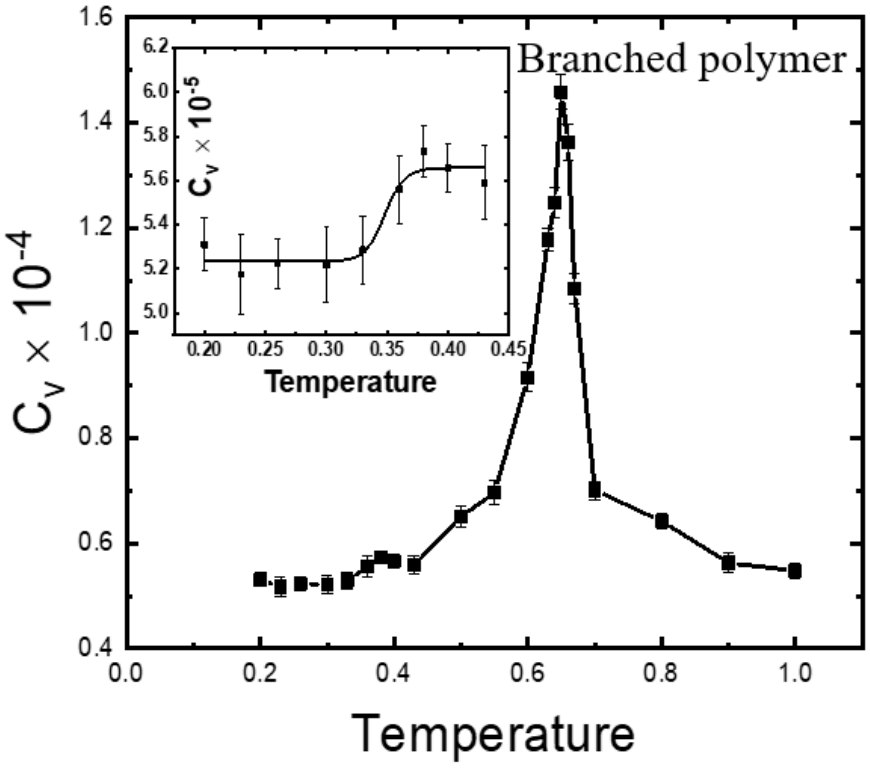

Figure 3. The heat capacity curve of (a) linear polymers (b) branched polymers. The melting temperature is identified in the main graph, while the glass transition temperature is revealed in the inset.

The semi-crystalline solid polymer is acquired as the temperature is below T_m. When the polymer is cooled further, small changes in the plots of both α-T and C_v-T curves can be identified again at a specific temperature about 0.38. Below this characteristic temperature, the degree of crystallinity is slightly increased in the α-T curve, while the heat capacity exhibits a sudden drop in the enlarged C_v-T curve (see the insets of Fig. 3). This change can be considered as the glass transition, which is known as a second-order phase transition. It is accompanied with no latent heat but a change in heat capacity, and thereby the glass-transition temperature is not easy to identify [67-69]. The temperature associated with the glass transition (T_g) is always lower than the melting temperature.

doi:10.6342/NTU202301105

When $T_m > T > T_g$, amorphous domains are distributed among crystalline domains, so-called the rubbery state, and thus solid polymers can be soft and flexible [70, 71]. However, as the temperature is below T_g, segmental motion in the amorphous portions of partially crystalline polymers are frozen, while the crystalline domain remains crystalline during the glass transition [72, 73]. Nonetheless, secondary crystallization proceeds even below T_g, leading to a more compact packing of aligned polymers [74]. Note that the difference of T_g between linear and branched polymers is difficult to distinguish in our model system.

According to the above analyses, the branched polymer has the melting temperature $T_m \approx 0.65$ and the glass-transition temperature $T_g \approx 0.38$. As a result, at $T = 0.5$, it is in the rubbery state and can be considered as an elastomer. The mechanical strength of the elastomer made of branched polymers can be strengthen by crosslinking [75-77]. The crosslinking degree is proportional to the concentration of crosslinkers and it is generally characterized by the gel content [78, 79]. Figure 4 shows the variation of the gel content with the crosslinker concentration (c_l). As expected, the gel content grows generally with increasing the crosslinker concentration, and it becomes 90% as $c_l = 2\%$. When the crosslinker concentration approaches around 3%, the gel content reaches 100%, indicating that all branched polymers in the system are crosslinked to form a network. In despite of the enhancement of the mechanical strength, it is known that crosslinking of polymers lessens the degree of crystallinity [16]. As shown in Fig. 4, the degree of crystallinity decreases with increasing the crosslinker concentration, because crosslinks act as defects to restrict the polymer motion and the development of alignment of chain segment [13, 80].

doi:10.6342/NTU202301105

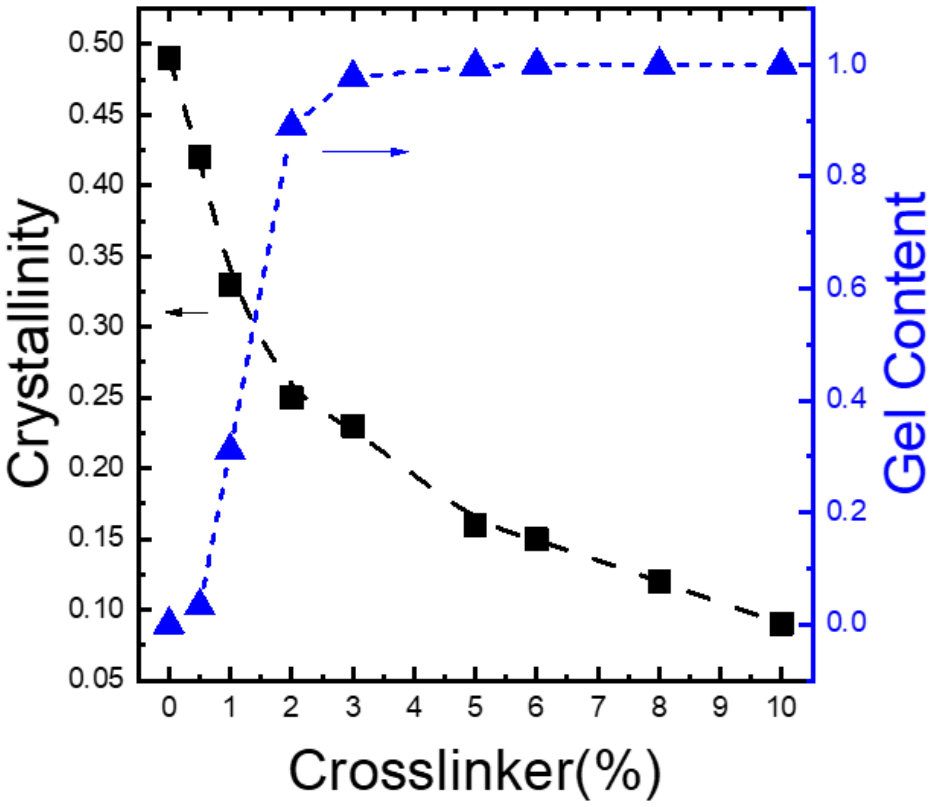

Figure 4. Effects of the crosslinking degree on the crystallinity and gel content.

3.2 Stress-strain relationship

It is known that the mechanical behavior of crosslinked polymers are primarily governed by crosslinking points [81]. Therefore, the mechanical properties are expected to depend on the crosslinker concentration. That is, the stress-strain curve which yields the information of Young's modulus (E), elongation at break, tensile strength, and toughness will be altered as the crosslinker concentration is changed. In this work, the crosslinking system of branched polymers is subjected to uniaxial stretch at a constant strain rate of 5×10^{-4} for the crosslinker concentration $c_l = 0.5$ - 10%.. Figure 5 shows some typical tensile stress-strain curves associated with different crosslinker concentrations at T = 0.5. The polymer system is in the rubbery state because $T_g < T <$

doi:10.6342/NTU202301105

T_m. Consistent with the experimental results for crosslinked polymers, a rather small increment of stress is observed at an ordinary strain but a rapid growth of stress appears as the strain approaches a critical value [82, 83]. Unlike the common stress-strain curve in which the maximum stress (tensile strength) occurs before reaching the elongation at break, the tensile strength of the crosslinking system is actually associated with the elongation at break without the presence of necking.

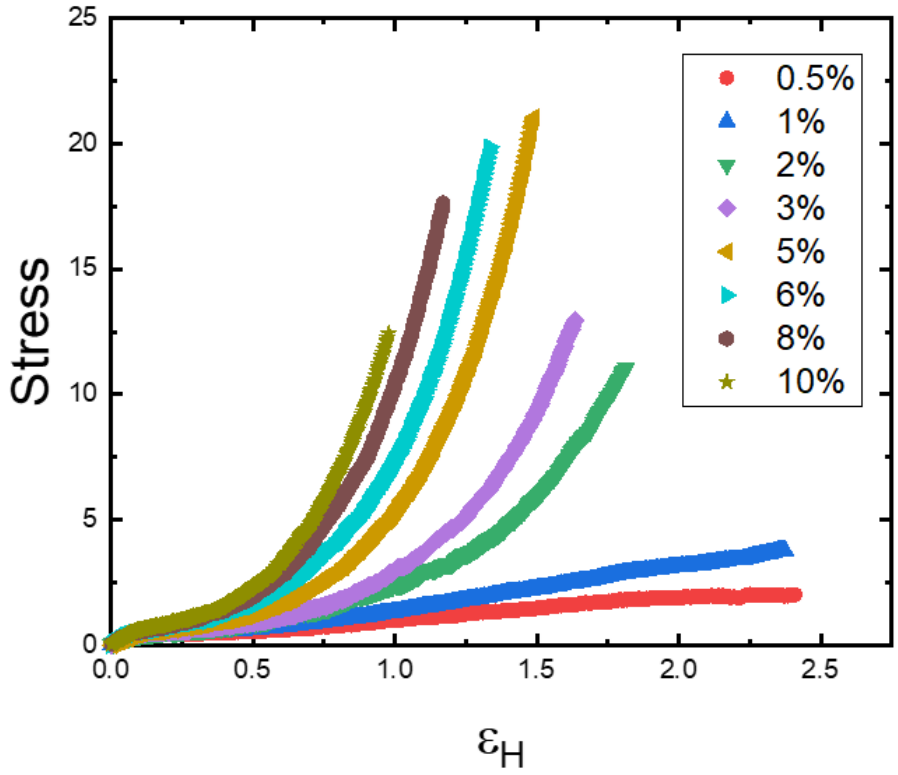

Figure 5. Tensile stress-strain curves associated with different crosslinker concentrations, where the Hencky (true) strain is used.

According to the stress-strain curve, Young's modulus can be determined from the slope of a linear fit to the curve within the Hencky strain of 3.6%, as shown in the inset of Fig. 6. The mean value of Young's modulus is acquired from ten stress-strain curves at a fixed crosslinker concentration. Figure 6 depicts the variation of Young's modulus

doi:10.6342/NTU202301105

with the crosslinker concentration, and it is found that E grows monotonously with increasing c_l. For crosslinked polymers with low crosslinker concentrations, the crosslinked structure is poorly connected. The primary resistance to small deformation is caused by entanglement and intermolecular sliding associated with the system without crosslinkers, leading to a low stiffness of the structure. In contrast, for higher concentrations of crosslinks, entanglement and sliding become limited owing to significant connectivity in the structure, and the deformation is mainly resisted by crosslinking points. Therefore, the higher the crosslinking degree, the stronger the crosslinked structure, corresponding to a higher stiffness of the structure [84].

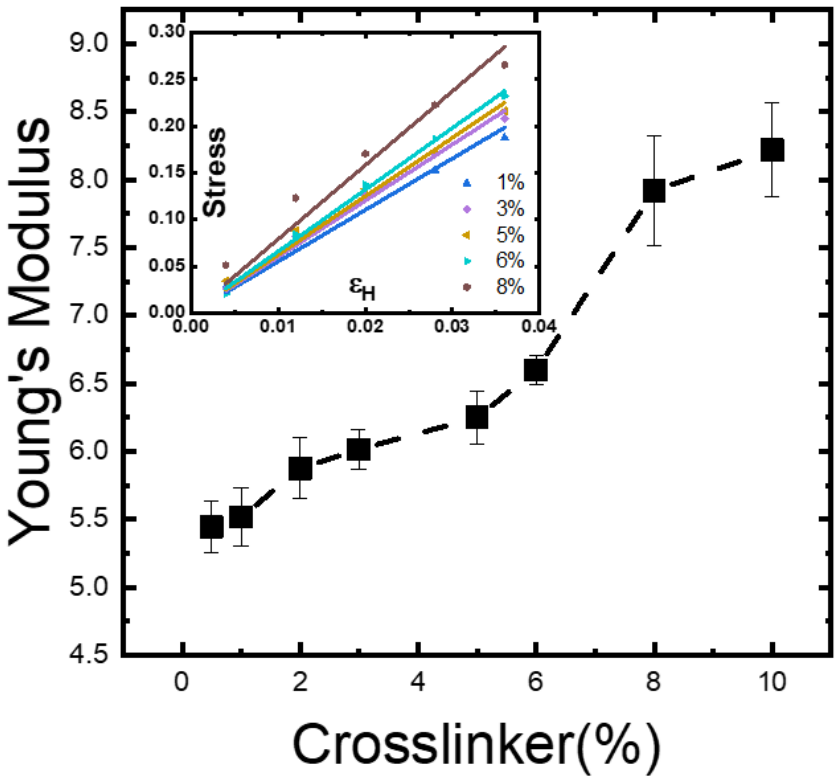

Figure 6. The variation of Young's modulus with the crosslinker concentration. The linearly elastic region of the stress-strain curve is shown in the inset.

doi:10.6342/NTU202301105

An important characteristic of elastomer is the large value of elongation at break. Figure 7a shows the variation of elongation at break with the crosslinker concentration. Opposite to Young's modulus, elongation at break decreases as the crosslinker concentration increases. Note that elongation at break in terms of Hencky strain from 98 to 241% is corresponding to that in terms of engineering strain from 166 to 1013%. The breakage of chemical bonds upon stretching can be avoided by chain elongation and intermolecular sliding. However, the increment of the crosslinking density results in a shorter segments available for elongation and a lower probability of chain slippage, leading to the decrement of elongation at break [23]. As the strain arrives at elongation at break, the stress reaches its maximum and the tensile strength is obtained. Unlike Young's modulus and elongation at break, the variation of the tensile strength with the crosslinker concentration is not monotonous, as demonstrated in Fig. 7b. The tensile strength is found to increase with c_l at low crosslinker concentrations but it becomes to decline at high concentrations. The maximum tensile strength occurs at $c_l \approx 5\%$. Similar to the tensile strength, the toughness of crosslinked polymers displays a non-monotonous variation with the crosslinker concentration as well. Its maximum also takes place at $c_l \approx 5\%$.

doi:10.6342/NTU202301105

(a)

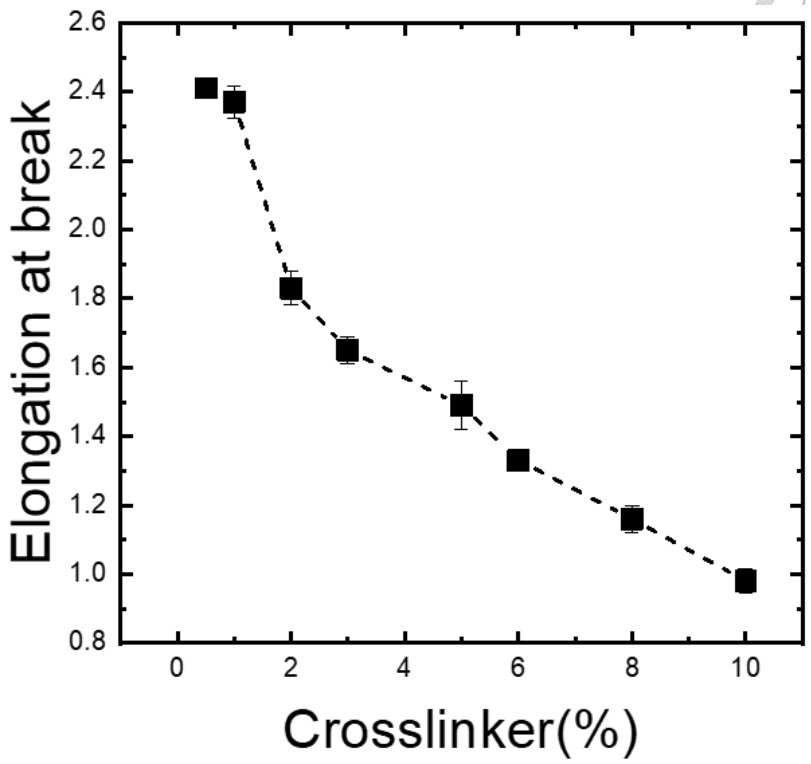

(b)

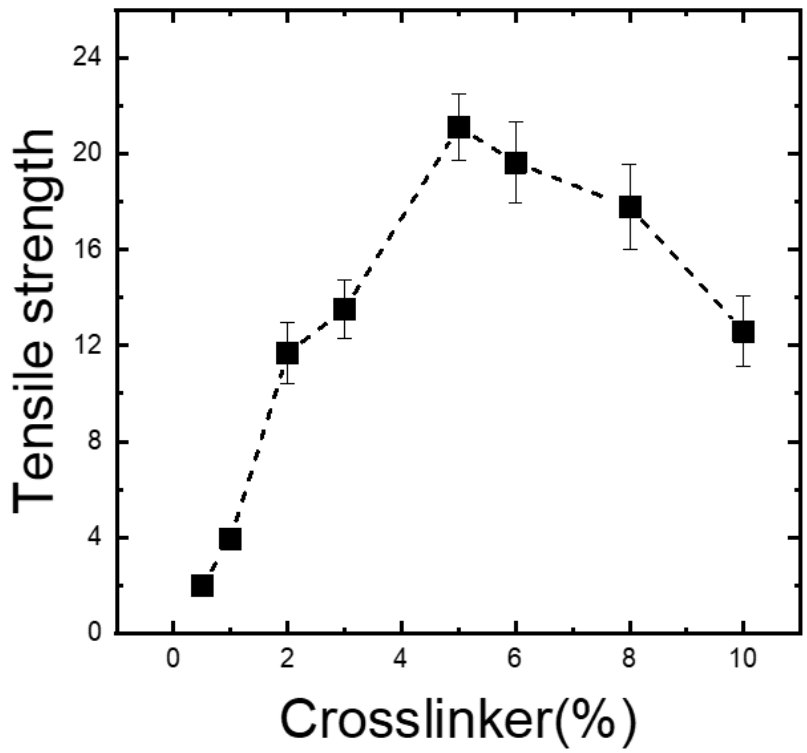

doi:10.6342/NTU202301105

(c)

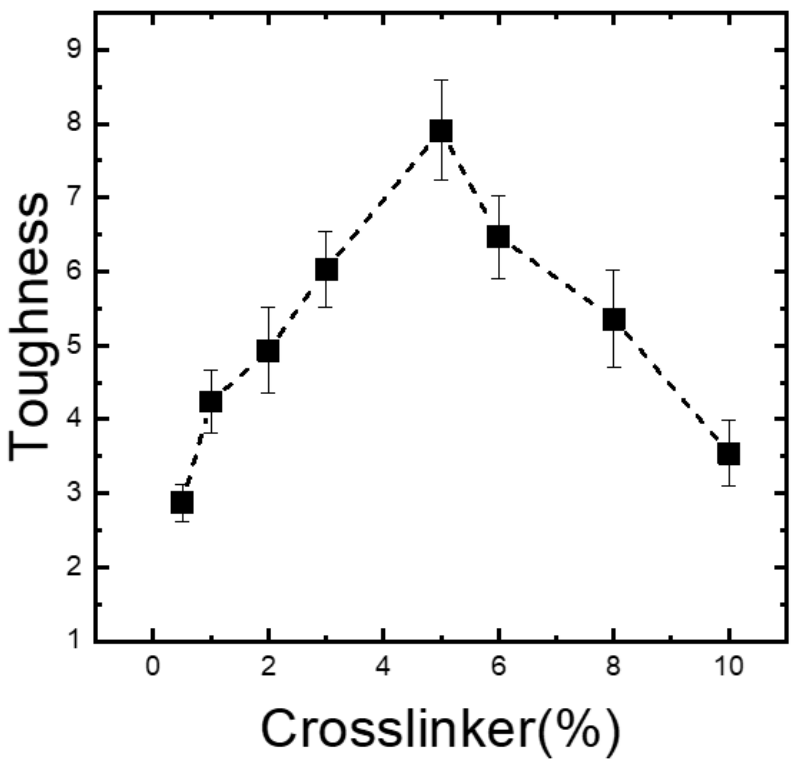

Figure 7. The variation of (a) elongation at break, (b) tensile strength, (c) toughness with the crosslinker concentration.

In addition to crosslinking points, the motion of polymers within the crosslinked network of elastomers is also restricted by chain entanglement [85]. The entanglement between two polymers results in a physical interlocking of polymer chains, which can lead to the formation of an intertwined network. Because entanglement of polymers hinders the movement of their segments, the rheology and mechanical properties of polymers are significantly affected, similar to the effect of crosslinking points [86]. In fact, entanglement acts as a slip link, which can increase the stiffness of the polymeric material and improve its tensile strength and toughness. Because the applied stress is dissipated by entangled polymers within a network, the polymer toughness can be enhanced [87]. However, unlike crosslinks, chain entanglement does not cause

doi:10.6342/NTU202301105

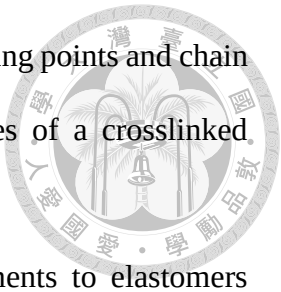

embrittlement of the polymer material [88]. Evidently, both crosslinking points and chain entanglements are crucial in determining the mechanical properties of a crosslinked elastomer.

The contributions of crosslinking points and chain entanglements to elastomers differ in certain mechanical properties, especially tensile strength and toughness. With an increase in crosslinking points within a network, the reptation of polymers and random motion of chain segments become more restricted, weakening the effect of chain entanglements. As a result, the competition between crosslinking points and chain entanglements gives each elastomer its unique mechanical characteristics. Recently, it has been reported that at low crosslinker concentrations, entanglements outnumber crosslinks and high toughness is obtained. In contrast, at high crosslinker concentrations, crosslinks become dominant over entanglements and eliminate the influence of chain entanglements, making the elastomer nearly brittle [24]. Additionally, the network's ability to dissipate input energy through molecular motion gradually diminishes, resulting in a decrease in tensile strength [89]. The aforementioned experimental results correspond to the simulation outcomes of $c_l \geq 5\%$ in Figs. 7b and 7c. The stiffness-toughness conflict becomes prominent with increasing c_l. On the contrary, for $c_l < 5\%$, the impact of crosslinking points on chain entanglements is limited and thus both tensile strength and toughness rise with increasing c_l.

3.3 Competition between crosslinking and entanglement

While the mechanical properties of crosslinked polymers can be directly measured in stretching experiments, observing their microstructural evolution presents a challenge. Coarse-grained molecular simulations, on the other hand, are able to capture the time-dependent microstructure of crosslinked polymers. It is known that the mechanical

doi:10.6342/NTU202301105

properties of crosslinked polymers are closely related to the structure and dynamics at the chain segment scale [90]. To simplify the analysis of microscopic changes in the polymer network during stretching, one can study the behavior of "individual" polymers in which the presence of crosslinks is disregarded. In this case, the effect of crosslinks can be seen as dynamic confinements that impact the stretching of bonds and polymer conformations. Figure 8a shows the average bond length ($\bar{l}_b^*$) and radius of gyration ($\bar{R}_g^*$) of those "individual" polymers of the crosslinked system at equilibrium. As demonstrated in the inset of Fig. 8a, the average bond length at equilibrium increases with higher crosslinker concentrations. Conversely, the average radius of gyration at equilibrium decreases with increasing crosslinker concentration, as shown in Fig. 8a. This finding suggests that the dynamical confinement associated with crosslinks actually has a different influence on the bond and chain length scales. With increased crosslinker concentration, the confinement domain decreases, causing a decrease in $\bar{R}_g^*$. However, to conform to the anisotropic confinements, the bonds have to stretch, leading to an increase in $\bar{l}_b^*$.

The changes in the microstructure of crosslinked polymers during stretching can also be observed by tracking the evolution of both $\bar{l}_b(t)$ and $\bar{R}_g(t)$. Figure 8b shows the relationship between average bond length and Hencky strain for different crosslinker concentrations. As expected, $\bar{l}_b$ always grows with increasing ε_H until it reaches the point of elongation at break. However, the average bond length increases at a faster rate for higher crosslinker concentrations. It is interesting to note that at higher crosslinker concentrations ($c_l \geq 5\%$), the network system breaks down when $\bar{l}_b$ reaches a similar limiting value ($\bar{l}_{b,limiting} \approx 0.565$), as illustrated in the inset of Fig. 8b. Because the effective equilibrium bond length ($\bar{l}_b^*$) is proportional to the crosslinker concentration, the observed outcome indicates that the stretching force that the bond can withstand actually

doi:10.6342/NTU202301105

decreases with increasing c_l. Conversely, when $c_l < 5\%$, the network system breaks down at $\bar{l}_{b,limiting}$ significantly lower than the limiting value observed in highly crosslinked systems, as shown in the inset of Fig. 8b. Interestingly, for the system without crosslinkers ($c_l = 0$), the point of elongation at break occurs at $\bar{l}_{b,limiting} \approx 0.4937$, only slightly beyond the effective equilibrium bond length $\bar{l}_b^* \approx 0.4887$.

While $\bar{l}_b(t)$ provides the evolution at the bond length level, $\bar{R}_g(t)$ can give the changes of the polymer network at the chain size level subjected to local confinement. Figure 8c shows the variation of $\bar{R}_g/\bar{R}_{g0}$ with Hencky strain for different crosslinker concentrations. For comparison, the upper left inset of Fig. 8c displays the change of $\bar{R}_g/\bar{R}_{g0}$ in the absence of crosslinkers. Here $\bar{R}_{g0} = \bar{R}_g^*(c_l = 0)$ is defined as the average radius of gyration without crosslinkers at equilibrium. As expected, $\bar{R}_g(t)$ always increases with an increasing Hencky strain, irrespective of the crosslinker concentration. However, the growth rate and the maximum value of the average radius of gyration with respect to the Hencky strain depend on the crosslinker concentration. The change of $\bar{R}_g$ with ε_H at higher crosslinker concentrations is more rapid than that at lower concentrations, even though the former has a smaller equilibrium value $\bar{R}_g(t = 0) = \bar{R}_g^*$ than the latter. This result suggests that for a higher degree of crosslinking, the elongation of the network is more easily distributed to chain stretching. However, the maximum value of $\bar{R}_g$ termed $\bar{R}_{g,max}$, which corresponds to the elongation at break, decreases with an increase in the crosslinker concentration as illustrated in the lower right inset of Fig. 8c. In accordance with the maximum bond length (see Fig. 8b), this consequence can be explained by the reason that the chains of a higher degree of crosslinking are stretched faster and reach the maximum bond length earlier, leading to a smaller $\bar{R}_g$ at break.

doi:10.6342/NTU202301105

(a)

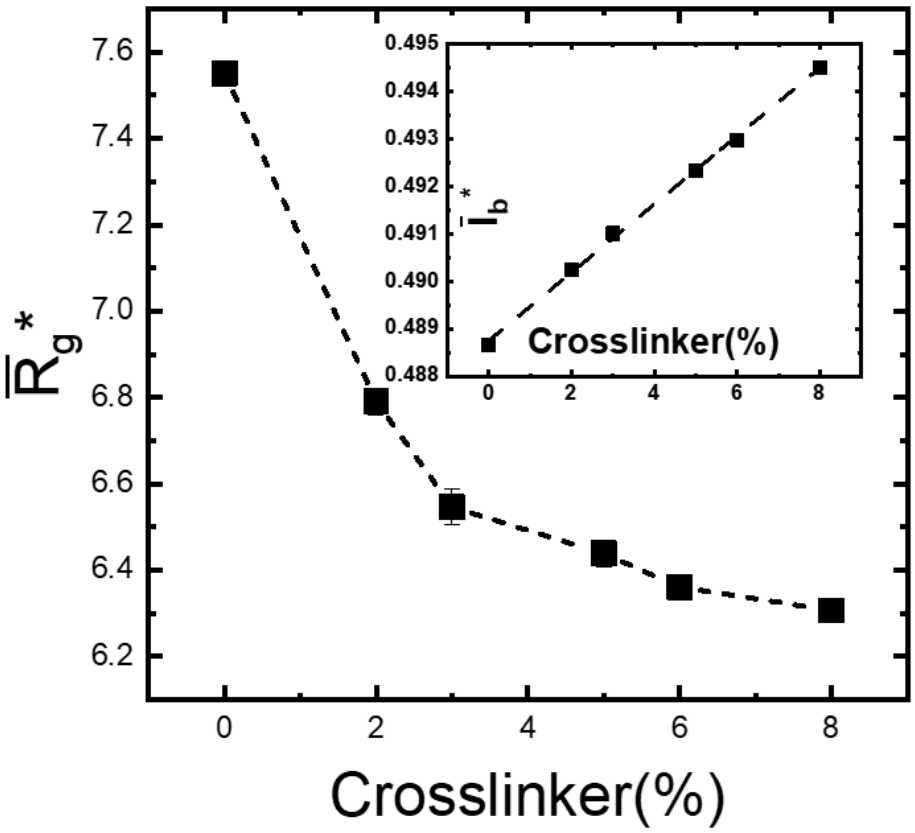

(b)

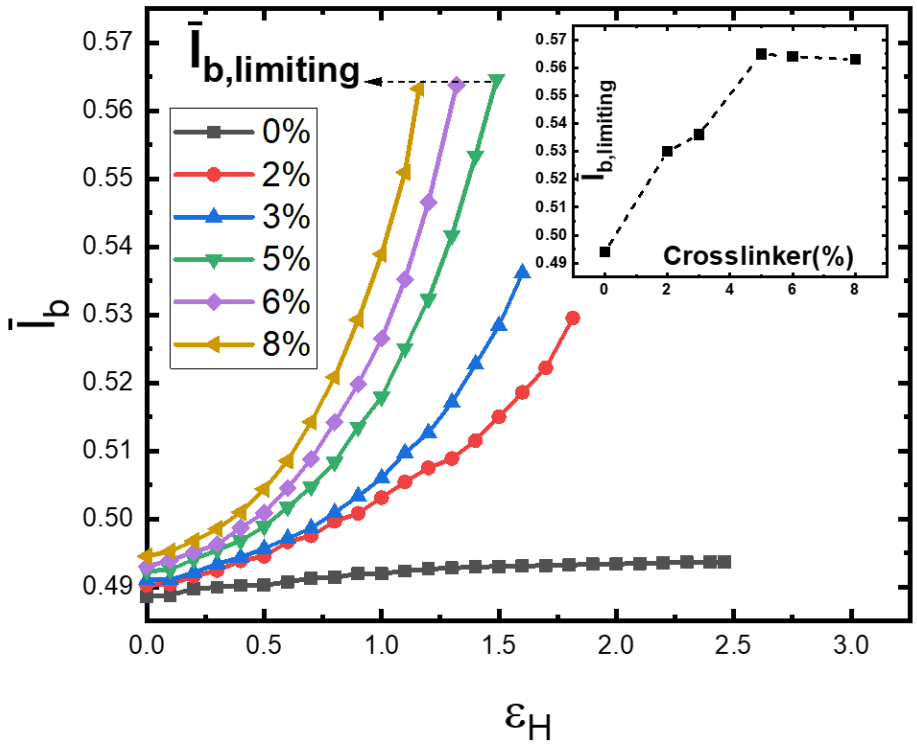

doi:10.6342/NTU202301105

(c)

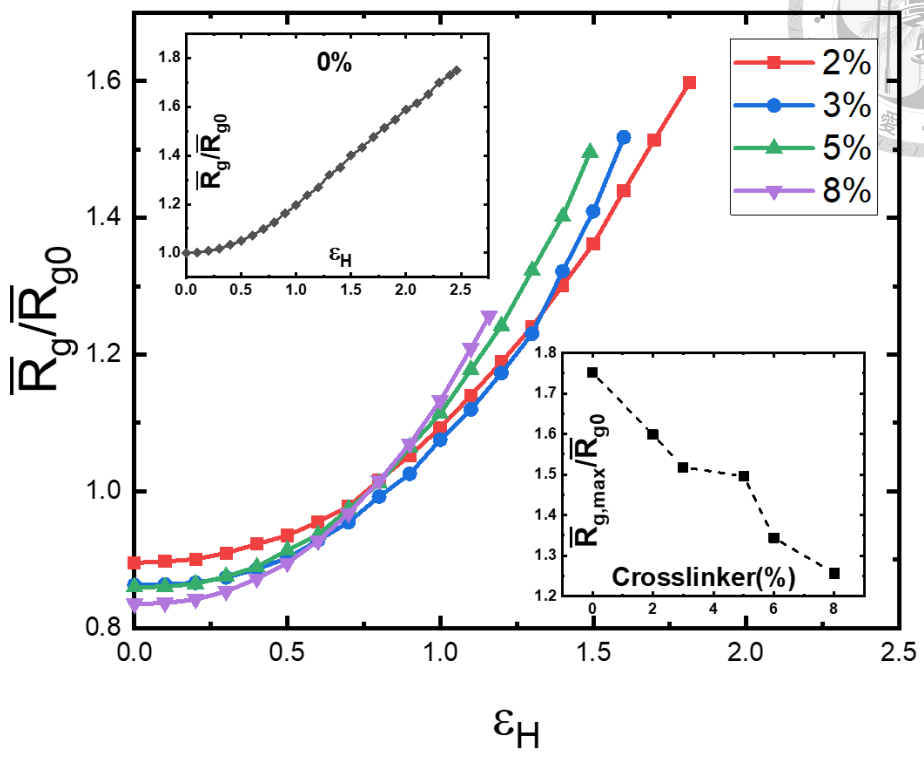

Figure 8. (a) The variation of the average radius of gyration with the crosslinker concentration at equilibrium. The average bond length is shown in the inset. (b) The relationship between the average bond length and Hencky strain for different crosslinker concentrations. The limiting value of $\overline{l}_b$ at break, $\overline{l}_{b,\,limiting}$, is shown in the inset. (c) The variation of the average radius of gyration with Hencky strain for different crosslinker concentrations. The result in the absence of crosslinkers is shown in the upper left inset. The $\overline{R}_{g,\,max}$ as a function of the crosslinker concentration is illustrated in the lower right inset.

There exist an optimal crosslinker concentration ($c_l \approx 5\%$) that yield the maximum tensile strength and toughness associated with the point of breakage, as indicated in Figs. 7b and 7c. This optimal concentration also corresponds to the specific crosslinker concentration at which the gel content reaches 100%, as shown in Fig. 4. Evidently, the

doi:10.6342/NTU202301105

crosslinker concentration alone is not enough to capture both the degree of crosslinking and chain entanglement. For $c_l \geq 5\%$, crosslinks are sufficient to uniformly withstand the stretching force at the bond length level, but the corresponding capability decreases at the chain size level. The former is referred to as the crosslinking effect revealed by $\bar{l}_b(t)$, while the latter is associated with chain entanglement indicated by $\bar{R}_g(t)$. As c_l exceeds the optimal concentration more, the crosslinking effect approaches saturation (see inset of Fig. 8b), but the contribution of chain entanglement weakens (see lower right inset of Fig. 8c), leading to a decrease in both tensile strength and toughness. On the contrary, when c_l is below 5%, the crosslinking effect increases (see inset of Fig. 8b) while chain entanglement decreases (see lower right inset of Fig. 8c) as the crosslinker concentration increases. The former effect dominates over the latter, resulting in an increase in both tensile strength and toughness. Our aforementioned analysis suggests that there exist two opposing contributions for tensile strength with increasing c_l. The optimal concentration arises from the competition between crosslinking and entanglement, as revealed by $\bar{l}_b(t)$ and $\bar{R}_g(t)$.

doi:10.6342/NTU202301105

Chapter 4 Conclusion

The effect of the crosslinking degree on the mechanical characteristics of the elastomer made of branched polymers are explored by dissipative particle dynamics simulations. As the concentration of crosslinker increases, the degree of crystallinity is found to decrease while the gel content increases, which is consistent with experimental findings. On the basis of the stress-strain curves obtained at different crosslinking degrees, the mechanical properties of the elastomers are determined, including Young's modulus, elongation at break, tensile strength, and toughness. As expected, Young's modulus increases in a monotonic manner with increasing crosslinker concentration, indicating an improved ability for crosslinked polymers to resist deformation. On the contrary, elongation at break decreases monotonically as the crosslinker concentration increases. Interestingly, it is found that the tensile strength and toughness of crosslinked polymers reach a peak value at the optimal concentration and then decrease steadily as the degree of crosslinking increases. This outcome can be attributed to the interplay between two opposing factors: crosslinking points and chain entanglements.

Molecular simulations can provide microscopic observations at the level of bond and chain lengths during the stretching process. Through monitoring the evolution of both average bond length $\bar{l}_b(t)$ and average radius of gyration of polymers $\bar{R}_g(t)$, the dynamics of the polymer network can be captured. While the former represents the influence of crosslinks, the latter illustrates the impact of entanglements. Both $\bar{l}_b$ and $\bar{R}_g$ increase with increasing strain ε_H, and their growth rates are faster for higher crosslinker concentrations. At rupture, the upper limit of $\bar{l}_b$ generally increases with the crosslinker concentration but it reaches a saturated value for concentrations exceeding the optimal concentration. On the contrary, the maximum value of $\bar{R}_g$ always decreases with

doi:10.6342/NTU202301105

increasing the crosslinker concentration. These results indicate that an increase in crosslinker concentration leads to greater crosslinking enhancement, but this effect eventually reaches a saturation point. Meanwhile, the contribution of chain entanglements continuously declines. As a result, beyond the optimal concentration, the combination of both chain crosslinking (level off) and entanglement (diminishment) effects result in a decrease in both tensile strength and toughness.

doi:10.6342/NTU202301105

REFERENCES

1. Dohrer, K. K., Hazlitt, L. G., & Whiteman, N. F. **(1988).** Short chain branching distribution of ULDPE. Journal of Plastic Film & Sheeting, 4(3), 214-226.
2. Fazeli, N., & Mehranpour, M. **(2012).** Effect of dimethyl formamide in the synthesis of linear low density polyethylene on its rheological properties. Polymer testing, 31(5), 671-676.
3. Breuil, P. A. R., Magna, L., & Olivier-Bourbigou, H. **(2015).** Role of homogeneous catalysis in oligomerization of olefins: Focus on selected examples based on group 4 to group 10 transition metal complexes. Catalysis Letters, 145, 173-192.
4. Pouzada, A. S., & Sergio Pouzada, A. **(2021).** Selection of thermoplastics. Design and Manufacturing of Plastics Products, 87-140.
5. Kontou, E., & Niaounakis, M. **(2006).** Thermo-mechanical properties of LLDPE/SiO2 nanocomposites. Polymer, 47(4), 1267-1280.
6. Bekhit, M., El-Sabbagh, S. H., Mohamed, R. M., El-Sayyad, G. S., & Sokary, R. **(2021).** Mechanical, Thermal and Antimicrobial Properties of LLDPE/EVA/MMT/Ag Nanocomposites Films Synthesized by Gamma Irradiation. Journal of Inorganic and Organometallic Polymers and Materials, 1-15.
7. Hashemi, S., & Williams, J. G. **(1986).** A fracture toughness study on low density and linear low density polyethylenes. Polymer, 27(3), 384-392.
8. Kulikov, O. **(2005).** Novel processing aids for extrusion of polyethylene. Journal of Vinyl and Additive Technology, 11(3), 127-131.
9. Constantin, D. **(1984).** Linear-low-density polyethylene melt rheology: Extensibility and extrusion defects. Polymer Engineering & Science, 24(4), 268-274.
10. Hojjati, M. R., Bassanajili, S., & Forootan, A. **(2018).** The Effect of Structural Parameters on the Cross-Linking of Various Grades of LLDPE. Iranian Journal of

doi:10.6342/NTU202301105

Chemistry and Chemical Engineering, 37(1), 175-183.

11. Kuan, H. C., Kuan, J. F., Ma, C. C. M., & Huang, J. M. **(2005).** Thermal and mechanical properties of silane-grafted water crosslinked polyethylene. Journal of applied polymer science, 96(6), 2383-2391.
12. Bermejo, J. S., & Ugarte, C. M. **(2009).** Influence of cross-linking density on the glass transition and structure of chemically cross-linked PVA: a molecular dynamics study. Macromolecular theory and simulations, 18(6), 317-327.
13. Liu, S. Q., Gong, W. G., & Zheng, B. C. **(2014).** The effect of peroxide cross-linking on the properties of low-density polyethylene. Journal of Macromolecular Science, Part B, 53(1), 67-77.
14. Patermann, S., & Altstädt, V. **(2015).** Influence of different crosslinking systems on the mechanical and morphological properties of thermoplastic vulcanizates. In AIP Conference Proceedings (Vol. 1664, No. 1, p. 120002). AIP Publishing LLC.
15. Wang, L., Shen, Y., Lai, X., Li, Z., & Liu, M. **(2011).** Synthesis and properties of crosslinked waterborne polyurethane. Journal of polymer research, 18, 469-476.
16. Ke, Q. Q., Huang, X. Y., Wei, P., Wang, G. L., & Jiang, P. K. **(2007).** Thermal, mechanical, and dielectric behaviors of crosslinked linear low density polyethylene/polyolefin elastomers blends. Journal of applied polymer science, 104(3), 1920-1927.
17. Isac, S., & George, K. E. **(2005).** Silane grafting of polyethylenes. International Journal of Polymeric Materials, 54(5), 397-413.
18. Ren, Y., Sun, X., Chen, L., Li, Y., Sun, M., Duan, X., & Liang, W. **(2021).** Structures and impact strength variation of chemically crosslinked high-density polyethylene: effect of crosslinking density. RSC advances, 11(12), 6791-6797.
19. Jiang, S., Yuan, C., Guo, Z., & Bai, X. **(2019).** Effect of crosslink on tribological

doi:10.6342/NTU202301105

performance of polyurethane bearing material. Tribology International, 136, 276-284.

20. Song, Y., Wang, L., Gyanda, R., Sakhuja, R., Cavallaro, M., Jackson, D. C., Meher, N. K., Ciaramitaro, D. A., Bedford, C. D., & Katritzky, A. R. **(2010).** Effect of the crosslink functionality on the mechanical properties of crosslinked 1, 2, 3-triazole polymers as potential binders for rocket propellants. Journal of applied polymer science, 117(1), 473-478.
21. Trzebiatowska, P. J., Echart, A. S., Correas, T. C., Eceiza, A., & Datta, J. **(2018)**. The changes of crosslink density of polyurethanes synthesised with using recycled component. Chemical structure and mechanical properties investigations. Progress in Organic Coatings, 115, 41-48.
22. Yussuf, A. A., Kosior, E., & Alban, L. **(2007).** Silane Grafting and Crosslinking of Metallocene-catalysed LLDPE and LDPE. Malaysian polymer journal, 2(2), 58-71.
23. Khonakdar, H. A., Morshedian, J., Wagenknecht, U., & Jafari, S. H. **(2003).** An investigation of chemical crosslinking effect on properties of high-density polyethylene. Polymer, 44(15), 4301-4309.
24. Kim, J., Zhang, G., Shi, M., & Suo, Z. **(2021).** Fracture, fatigue, and friction of polymers in which entanglements greatly outnumber cross-links. Science, 374(6564), 212-216.
25. Li, C., & Strachan, A. **(2015).** Molecular scale simulations on thermoset polymers: A review. Journal of polymer science part B: polymer physics, 53(2), 103-122.
26. Espanol, P., & Warren, P. B. **(2017).** Perspective: Dissipative particle dynamics. The Journal of chemical physics, 146(15), 150901.
27. Groot, R. D., & Warren, P. B. **(1997).** Dissipative particle dynamics: Bridging the gap between atomistic and mesoscopic simulation. The Journal of chemical physics, 107(11), 4423-4435.

doi:10.6342/NTU202301105

28. Wei, T., & Ren, C. **(2020).** Theoretical simulation approaches to polymer research. In Polymer science and innovative applications (pp. 207-228). Elsevier.
29. Liu, M. B., Liu, G. R., Zhou, L. W., & Chang, J. **(2015).** Dissipative particle dynamics (DPD): an overview and recent developments. Archives of Computational Methods in Engineering, 22, 529-556.
30. Groot, R. D., & Rabone, K. L. **(2001).** Mesoscopic simulation of cell membrane damage, morphology change and rupture by nonionic surfactants. Biophysical journal, 81(2), 725-736.
31. Li, Z., Bian, X., Caswell, B., & Karniadakis, G. E. **(2014).** Construction of dissipative particle dynamics models for complex fluids via the Mori–Zwanzig formulation. Soft Matter, 10(43), 8659-8672.
32. Hsieh, M. C., Tsao, Y. H., Sheng, Y. J., & Tsao, H. K. **(2023).** Microstructural Dynamics of Polymer Melts during Stretching: Radial Size Distribution. Polymers, 15(9), 2067.
33. Alvarez, F., Flores, E. A., Castro, L. V., Hernández, J. G., López, A., & Vazquez, F. **(2011).** Dissipative particle dynamics (DPD) study of crude oil− water emulsions in the presence of a functionalized co-polymer. Energy & fuels, 25(2), 562-567.
34. Xiao, S., Chen, H. Y., Sheng, Y. J., & Tsao, H. K. **(2015).** Induced polar order in sedimentation equilibrium of rod-like nanoswimmers. Soft Matter, 11(12), 2416-2422.
35. Avalos, J. B., & Mackie, A. D. **(1997).** Dissipative particle dynamics with energy conservation. Europhysics Letters, 40(2), 141.
36. Yang, Y. L., Tsao, H. K., & Sheng, Y. J. **(2020).** Morphology and Wetting Stability of Nanofilms of ABC Miktoarm Star Terpolymers. Macromolecules, 53(2), 594-601.
37. Chu, K. C., Tsao, H. K., & Sheng, Y. J. **(2020).** Pressure-gated capillary nanovalves

doi:10.6342/NTU202301105

based on liquid nanofilms. Journal of colloid and interface science, 560, 485-491.

38. Ni, T., Huang, G. S., Gao, P., Xu, Y. T., & Yang, M. Z. **(2011).** Dissipative particle dynamics simulation on the association properties of fluorocarbon-modified polyacrylamide copolymers. Polymer journal, 43(7), 635-641.
39. Pan, D., Hu, J., & Shao, X. **(2016).** Lees–Edwards boundary condition for simulation of polymer suspension with dissipative particle dynamics method. Molecular Simulation, 42(4), 328-336.
40. Singh, A., Chakraborti, A., & Singh, A. **(2018).** Role of a polymeric component in the phase separation of ternary fluid mixtures: a dissipative particle dynamics study. Soft Matter, 14(21), 4317-4326.
41. Thompson, A. P., Aktulga, H. M., Berger, R., Bolintineanu, D. S., Brown, W. M., Crozier, P. S., in't Veld, P. J., Kohlmeyer, A., Moore, S. G., & Nguyen, T. D. **(2022).** LAMMPS-a flexible simulation tool for particle-based materials modeling at the atomic, meso, and continuum scales. Computer Physics Communications, 271, 108171.
42. Rudin, A., & Choi, P. **(2012).** The elements of polymer science and engineering. Academic press.
43. McKeen, L. W. (2018). The effect of sterilization on plastics and elastomers. William Andrew.
44. Oyama, T. **(2015).** Cross-Linked Polymer Synthesis. In S. Kobayashi & K. Müllen (Eds.), Encyclopedia of Polymeric Nanomaterials (pp. 496-505). Springer Berlin Heidelberg.
45. Nikunen, P., Vattulainen, I., & Karttunen, M. **(2007).** Reptational dynamics in dissipative particle dynamics simulations of polymer melts. Physical Review E, 75(3), 036713.

doi:10.6342/NTU202301105

46. Jabbari-Farouji, S., Rottler, J., Lame, O., Makke, A., Perez, M., & Barrat, J. L. **(2015).** Plastic deformation mechanisms of semicrystalline and amorphous polymers. ACS Macro Letters, 4(2), 147-150.
47. Liu, X., Luo, J., Yin, N., Tan, Z. C., & Shi, Q. **(2018).** Applications of low temperature calorimetry in material research. Chinese Chemical Letters, 29(5), 664-670.
48. Phillips, J., Isgro, T., Sotomayor, M., & Villa, E. **(2003).** NAMD TUTORIAL.
49. Skačej, G., & Zannoni, C. **(2011).** Main-chain swollen liquid crystal elastomers: a molecular simulation study. Soft Matter, 7(21), 9983-9991.
50. Chang, H. Y., Sheng, Y. J., & Tsao, H. K. **(2022).** Packing microstructures and thermal properties of compressed emulsions: Effect of droplet size. Journal of Molecular Liquids, 364, 120025.
51. Romani, F., Corrieri, R., Braga, V., & Ciardelli, F. **(2002).** Monitoring the chemical crosslinking of propylene polymers through rheology. Polymer, 43(4), 1115-1131.
52. Narkis, M., Raiter, I., Shkolnik, S., Siegmannz, A., & Eyerer, P. **(1987).** Structure and tensile behavior of irradiation-and peroxide-crosslinked polyethylenes. Journal of Macromolecular Science—Physics, 26(1), 37-58.
53. Karatrantos, A., Composto, R. J., Winey, K. I., & Clarke, N. **(2011).** Structure and conformations of polymer/SWCNT nanocomposites. Macromolecules, 44(24), 9830-9838.
54. Wang, Y., Liu, H., Li, P., & Wang, L. **(2022).** The Effect of Cross-Linking Type on EPDM Elastomer Dynamics and Mechanical Properties: A Molecular Dynamics Simulation Study. Polymers, 14(7), 1308.
55. Sliozberg, Y. R., Chantawansri, T. L., Lenhart, J. L., & Andzelm, J. W. **(2014).** Structural and mechanical properties of advanced polymer gels with rigid side-chains using coarse-grained molecular dynamics. Polymer, 55(20), 5266-5275.

doi:10.6342/NTU202301105

56. Jiang, T., Wang, L., & Lin, J. **(2013).** Mechanical properties of designed multicompartment gels formed by ABC graft copolymers. Langmuir, 29(39), 12298-12306.
57. Mai-Duy, N., Phan-Thien, N., & Khoo, B. C. **(2015).** Investigation of particles size effects in dissipative particle dynamics (DPD) modelling of colloidal suspensions. Computer Physics Communications, 189, 37-46.
58. Palomba, D., Vazquez, G. E., & Díaz, M. F. **(2014).** Prediction of elongation at break for linear polymers. Chemometrics and Intelligent Laboratory Systems, 139, 121-131.
59. Chen, E. J., Novakofski, J., Jenkins, W. K., & O'Brien, W. D. **(1996).** Young's modulus measurements of soft tissues with application to elasticity imaging. IEEE Transactions on ultrasonics, ferroelectrics, and frequency control, 43(1), 191-194.
60. Yubo, T. A. O., Peng, L. I., & Ling, P. A. N. **(2020).** Improving tensile properties of polylactic acid parts by adjusting printing parameters of open source 3D printers. Materials Science, 26(1), 83-87.
61. Marar, K., Eren, Ö., & Celik, T. **(2001).** Relationship between impact energy and compression toughness energy of high-strength fiber-reinforced concrete. Materials letters, 47(4-5), 297-304.
62. Shan, C. L. P., Soares, J. B. P., & Penlidis, A. **(2002).** Mechanical properties of ethylene/1-hexene copolymers with tailored short chain branching distributions. Polymer, 43(3), 767-773.
63. Poongavalappil, S., Svoboda, P., Theravalappil, R., Svobodova, D., Ougizawa, T., & Sedlacek, T. **(2013).** Influence of branching density on the cross-linkability of ethylene-octene copolymers. Polymer journal, 45(6), 651-658.
64. Rocha, M. C. G., Leyva, M. E., & Oliveira, M. G. D. **(2014).** Thermoplastic elastomers blends based on linear low density polyethylene, ethylene-1-octene

doi:10.6342/NTU202301105

copolymers and ground rubber tire. Polímeros, 24, 23-29.

65. Sheng, Y. J., Lin, H. J., Chen, J. Z., & Tsao, H. K. **(2004).** Static properties of a stacking chain. Macromolecules, 37(25), 9631-9638.
66. Sheng, Y. J., Mou, Y. C., & Tsao, H. K. **(2006).** Conformational entropy of a pseudoknot polymer. The Journal of chemical physics, 124(12), 124904.
67. Roos, Y. H. **(2009).** Mapping the different states of food components using state diagrams. In Modern Biopolymer Science (pp. 261-276). Elsevier.
68. Wu, J. **(1999).** The glassy state, ideal glass transition, and second-order phase transition. Journal of applied polymer science, 71(1), 143-150.
69. Wunderlich, B. **(2007).** Glass transition as a key to identifying solid phases. Journal of applied polymer science, 105(1), 49-59.
70. Somwanshi, S. B., Dolas, R. T., Wagh, V. D., & Kotade, K. B. **(2016).** Pharmaceutically used plasticizers: a review. Eur. J. Biomed. Pharm. Sci, 3, 277-285.
71. Sun, L., Huang, W. M., Wang, C. C., Zhao, Y., Ding, Z., & Purnawali, H. **(2011).** Optimization of the shape memory effect in shape memory polymers. Journal of Polymer Science Part A: Polymer Chemistry, 49(16), 3574-3581.
72. Hess, M., Allegra, G., He, J., Horie, K., Kim, J.-S., Meille, S. V., Metanomski, V., Moad, G., Stepto, R. F., & Vert, M. **(2013).** Glossary of terms relating to thermal and thermomechanical properties of polymers (IUPAC Recommendations 2013). Pure and Applied Chemistry, 85(5), 1017-1046.
73. Huo, P., & Cebe, P. **(1992).** Temperature-dependent relaxation of the crystal-amorphous interphase in poly (ether ether ketone). Macromolecules, 25(2), 902-909.
74. Bagher, A. M., & Reza, B. M. **(2015).** Polymer Optic Technology. Optics, 4(1), 1.
75. Maitra, J., & Shukla, V. K. **(2014).** Cross-linking in hydrogels-a review. Am. J. Polym. Sci, 4(2), 25-31.

doi:10.6342/NTU202301105

76. Chua, J., & Tu, Q. **(2018).** A molecular dynamics study of crosslinked phthalonitrile polymers: the effect of crosslink density on thermomechanical and dielectric properties. Polymers, 10(1), 64.
77. Martinez, A. W., Caves, J. M., Ravi, S., Li, W., & Chaikof, E. L. **(2014).** Effects of crosslinking on the mechanical properties, drug release and cytocompatibility of protein polymers. Acta biomaterialia, 10(1), 26-33.
78. Kampouris, E. M., & Andreopoulos, A. G. **(1989).** Gel content determination in cross-linked polyethylene. Biomaterials, 10(3), 206-208.
79. Kopač, T., Ručigaj, A., & Krajnc, M. **(2020).** The mutual effect of the crosslinker and biopolymer concentration on the desired hydrogel properties. International journal of biological macromolecules, 159, 557-569.
80. Peng, H., Lu, M., Lv, F., Niu, M., & Wang, W. **(2019).** Understanding the effect of silane crosslinking reaction on the properties of pp/poe blends. Polymer Bulletin, 76, 6413-6428.
81. Xu, L., Qiao, Y., & Qiu, D. **(2023).** Coordinatively Stiffen and Toughen Hydrogels with Adaptable Crystal-domain Cross-linking. Advanced Materials, 2209913.
82. Mark, J. E. **(2017).** Thermoset elastomers. In Applied Plastics Engineering Handbook (pp. 109-125). Elsevier.
83. Wang, Y., Gan, H.-L., Liang, C.-X., Zhang, Z.-Y., Xie, M., Xing, J.-Y., Xue, Y.-H., & Liu, H. **(2021).** Network structure and properties of crosslinked bio-based epoxy resin composite: An in-silico multiscale strategy with dynamic curing reaction process. Giant, 7, 100063.
84. Depalle, B., Qin, Z., Shefelbine, S. J., & Buehler, M. J. **(2015).** Influence of cross-link structure, density and mechanical properties in the mesoscale deformation mechanisms of collagen fibrils. Journal of the mechanical behavior of biomedical

doi:10.6342/NTU202301105

materials, 52, 1-13.

85. Mishra, S., Maiti, S., Pandey, P., & Rai, B. **(2021).** Effect of entanglement and crosslinking on the hyperelastic behavior of SBR rubber: A multiscale DPD simulation study.
86. Kong, D. C., Yang, M. H., Zhang, X. S., Du, Z. C., Fu, Q., Gao, X. Q., & Gong, J. W. **(2021).** Control of polymer properties by entanglement: a review. Macromolecular Materials and Engineering, 306(12), 2100536.
87. Norioka, C., Inamoto, Y., Hajime, C., Kawamura, A., & Miyata, T. **(2021).** A universal method to easily design tough and stretchable hydrogels. NPG Asia Materials, 13(1), 34.
88. Yuan, Z., Cao, Z., Ma, C., Wu, R., Wu, H., Xu, Q., Zheng, J., & Wu, J. **(2022).** Ultra-robust, repairable and smart physical hydrogels enabled by nano-domain reconfiguration of network topology. Chemical Engineering Journal, 450, 138085.
89. Joseph, A. M., Presannan, N., & Madhusoodanan, K. N. **(2017).** Mechanical devulcanization of carbon black filled natural rubber vulcanizates: effect of crosslink density. Rubber Sci, 30, 169-180.
90. Shen, J., Lin, X., Liu, J., & Li, X. **(2018).** Effects of cross-link density and distribution on static and dynamic properties of chemically cross-linked polymers. Macromolecules, 52(1), 121-134.

doi:10.6342/NTU202301105